JSEE Vol. 22, No. 3, 2020 DOI:10.48303/jsee.2020.251305

Research Paper

Material Weight and Constructability Optimization of Multifunction Earthquake Resilient Structures

Siavash Sedighi[1], Mark Grigorian[2], Marzieh Ansari Targhi[3], and Razieh Ansari Targhi[4]*

1. Ph.D. Candidate, Structural Engineering Department, Science and Research Branch, Islamic Azad University, Tehran, Iran, ORCID: 0000-0003-3066-5479,
*Corresponding Author; email: siavash.sedighi@srbiau.ac.ir
2. D.Phil., MGA Structural Engineering Consultants Inc., ORCID: 0000-0002-8508-1481
3. M.Sc. Graduate, Earthquake Engineering Department, Faculty of Engineering, University of Science and Culture, Tehran, Iran, ORCID: 0000-0003-0987-4241
4. M.Sc. Graduate, Earthquake Engineering Department, Faculty of Engineering, University of Science and Culture, Tehran, Iran, ORCID: 0000-0001-5710-8387

Received: 19/11/2021
Accepted: 04/04/2022

ABSTRACT

Optimization of sustainable seismic design (SSD) of building structures has been one of the most challenging and ongoing research subjects in the earthquake and structural engineering worldwide during the past ten years. The purpose of the current research article is to supplement recently developed concepts of sustainable seismic design of building structures through the limitation of damage, repairability, purpose-specific detailing, form optimization, material, and construction optimization, and development of practical technologies to achieve cost-efficient construction and post-earthquake realignment and repairs (PERR). Earthquake resisting moment frames of minimum-weight have been introduced as essential parts of SSD. Global stiffness reduction (GSR) and restoring force adjustment (RFA) concepts have been introduced to facilitate post-earthquake realignment and repairs. The rocking core-moment frame (RCMF) is the key part of the archetype in combination with other structural systems. SSD is a concept that requires a thorough appreciation of the mechanics of structural optimization, sequential failures, recentering, and earthquake-induced P-delta and residual effects. Article results show utilizing the proposed archetype can provide sustainability as well as weight and construction optimization. The archetype components are one of the conventional structural systems with no significant change in the construction procedure. Several cases have been discussed in detail to illustrate the applications of the proposed concepts.

Keywords:
Structural optimization; Seismic sustainability; Damage control; Realignment; Repairability; Minimum weight; Rocking core

1. Introduction

several authors [1-4] studied the Optimization of topologies, material consumption, and cost-effectiveness of different types of multidisciplinary or multifunctional engineering systems. However, optimization of SSD, being a relatively new field of research, has not been reported in the scientific media.

Optimization of SSD is a relatively new idea that was inspired by recent advances in Earthquake Engineering. Examples are "The Stiff Columns" [5], "Displacement Based Seismic Design (DBSD)" [6], "Real-Time Pseudo Dynamic Testing" [7], "Rocking Frames" [8] and the need to overcome large residual deformations due to major seismic events [9-10]. In the present context, SSD is a direct reference to the ability of a structure to either overcome large

post-earthquake residual deformations and P-delta effects or to lend itself well to other means of realignment. These innovations are brought together through performance control (PC) to develop a basis for the practical design of cost-effective, sustainable earthquake-resisting systems (ERSs). It has been shown, amongst others by Hajjar et al. [11] and Pollino et al. [12], that adequately designed "stiff columns" also known as "strong backs" and "rigid cores" [13] can improve the seismic response of conventional ERS. It has been shown [14-15] that stiff columns and similar systems can also be instrumental in recentering structures damaged by earthquakes. Here pre-tensioned rigid rocking cores (RRCs) are utilized to absorb seismic energies, suppress higher modes of vibrations, prevent soft story failure, induce uniform drift and facilitate the PERR process. By definition, in a rigid rocking core, the core rigidity ratio to the ERS is infinity. It has also been reported that earthquake-induced large residual displacements inhibit cost-effective repairs of damaged bridge columns and similar structures [16]. The same phenomenon is true for building structures with large numbers of earthquake-resisting elements. Instead of looking at residual deformations from an analysis and design point of view, the authors propose to confine residual effects to pre-designated, replaceable links or elements. Material optimization and construction economy have been achieved through analytic reasoning rather than numerical computations.

It is instructive to note that the high rigidity of the cores causes the initial and final mode shapes to remain the same during the history of loading of the structure. DBSD offers a consistent approach with the functional characteristics of the proposed system. SSD is a multi-objective concept with a view to life safety, physical collapse prevention, construction economy, and PERR. Currently, no code-sanctioned building structure can fulfill these criteria unless it has been designed, optimized, and detailed for the purpose. SSD uses the possibilities offered by rigid rocking cores, removal of residual effects, and the strategies involved in DBSD to develop archetypes that meet the proposed resiliency requirements. Therefore, the challenge is how to postulate and control desired damage patterns to achieve SSD. Almost all current seismic codes are based on the severity of structural components damage due to anticipated seismic activities. Here an attempt is made to extend the benefits of damage assessment to SSD with a view to structural Optimization, collapse prevention (CP), and PERR. The study of failure mechanisms of building frames becomes even more meaningful when their modes of occurrence are looked upon as instruments of feedback [17-18] and design rather than objectives. In SSD, the ability of the system to realign itself after a major earthquake is as essential as its capacity to resist the same earthquake without becoming disposable. This article is based on a simple methodology with a paradigm shift that entails new detailing and performance requirements for loading, unloading, and realignment stages of structures that sustain controlled damage due to recurring earthquakes. The importance of damage appraisal and proper detailing of self-centering systems has been discussed by [8, 14, 19].

Essential elements of SSD include accurate damage assessment, cost-effectiveness, and purpose-oriented detailing. Recently there have been many studies for developing new solutions such as structural dampers [20-21], replaceable ductility-providing fuses for earthquake resisting systems, such as Slip Friction Joints, Steel Shear Yielding Fuses, and replaceable moment connections, e.g., [22-23]. Although most of these innovative sub-systems and elements have passed actual tests and a wide range of time-history analyses, the structural functionality cannot be guaranteed after an earthquake unless the entire system has been designed to prevent physical collapse and efficiently lend itself to practical PERR. Despite these remarkable achievements and developments, the current design codes are not addressing the post-earthquake response of buildings, including the conditions for gravity structure, non-structural items, failure modes, residual deformations, or the required restoring forces. However, both the lawmakers as well as the engineering community have been expanding the discussions to reach workable frameworks of SSD [11, 15, 24, 25]. This article considers both the theoretical and practical aspects of SSD. To emphasize the physical aspects of the concept, simple elastoplastic force-displacement diagrams are discussed to reduce the cumbersome computations

to arithmetic combinations of idealized response curves.

Furthermore, the proposed design mainly relies on minor and straightforward modifications of conventional structural systems details and specifications. Through this idea, damage does not necessarily involve physical failure but rather elastoplastic energy dissipation at maximum design level demands. The validity and precision of provided cases have been verified by computer analysis through reliable software. The rocking core-moment frame (RCMF) combinations cited in this article have passed tests of experimentations as well as time history analysis. Extensive computer analysis support the viability of the parametric cases presented in this paper. All symbols are defined as they first appear in the text.

1.1. Study Goals and Organization

Theoretical analysis of several individual SS systems has been reported by [21-22, 24, 26]. The material presented in this paper flows from a brief introduction of the subject matter to the utilization of lessons learned from contemporary research to the development of practical design strategies, and eventually, to material optimization and detailing. Brief discussions of SSD basics and the development of the proposed archetype are presented in sections 2 and 3. Sections 4 and 5 deal with the design of the essential components of the system. In section 3.2, after developing the governing response equation of the imaginary module of regular MFs, the basic rules of minimum drift-minimum weight association are presented. The economics and optimization of SS structures are discussed in some length in section 6. Finally, section 7 utilizes incremental elastoplastic displacement analysis principles to provide a basis for diagrammatic presentation of the response of the proposed archetype. The essence of the current article is illustrated by the following SDOF simple case that attempts to extend the applications of damage control to PERR.

2. SSD Basics

In general, seismically sustainable (SS) archetypes consist of three separate structures, connected in parallel, with distinct operational functions. A perfectly articulated gravity framing that neither resists earthquakes nor impedes the recentering process, a code sanctioned ERS and a stabilized RRC with or without supplementary devices. Figures (1a) and (2a) represent one such system under gravity and lateral forces P and $\pm V$ respectively. The subject model consists of an upright wide flange cantilever of stiffness K_F, plastic moment of resistance M^P with effective mass $m_e = W / g$ that

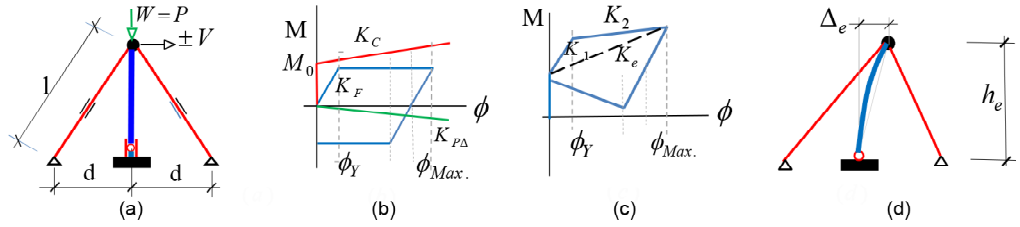

Figure 1. (a) Symbolic SDOF structure, (b) Individual response plots, where and stand for yield and maximum drift ratios respectively, (c) Stabilized, partial hysteresis plot of the combined structure, and (d) Post-damage equilibrium state with a plastic hinge at the base level.

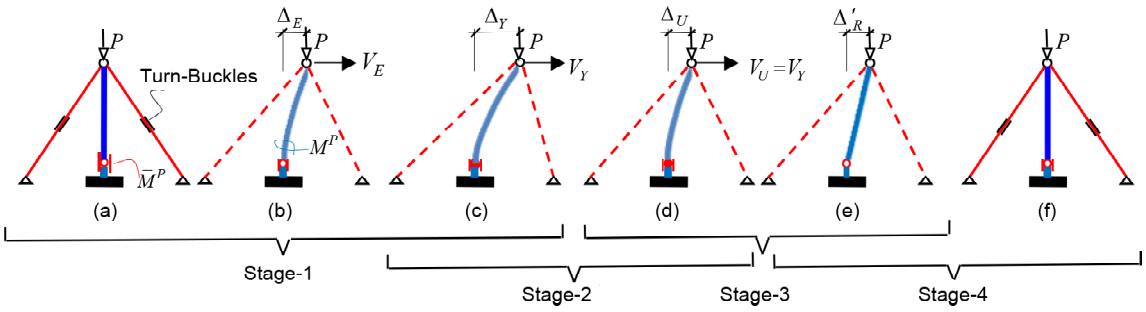

Figure 2. (a) Symbolic structure, (b) Linear response, (c) First yield, (d) Ultimate loading, (e) unloading, flange plates removed, and (f) system recentered, new flange plates installed.

symbolizes a moment frame, connected to its base utilizing a replaceable energy dissipating moment connection (REDMC), with $\bar{M}^P < M^P$, where $\bar{M}^P$ denotes the REDMC and a pair of pre-loaded high strength cables with total stiffness $K_C = 2K_T$, (K_T is the stiffness of any one of the stretched cables) equipped with standard turnbuckles and pre-loaded to produce an elastic moment of resistance when the leeward cable is detensioned. The symbolic structure is an SDOF system and causes its components to absorb proportional amounts of energies [27]. Consequently, the force-deformation relationships of the members of the combined system can be expressed in terms of a single variable $\varphi = \Delta / h_e$, where Δ represents lateral displacement at cantilever height h_e. As precautionary measures, both cables are designed for unlikely conditions, $M_0 \to 0$, where K_C reduces to $K_C = K_T$ after both the cantilever and the leeward cable become incapacitated. Here an assumption is made that the system will remain stable and sustain large lateral displacements after forming a base level plastic hinge and that $M_0 > 0$.

2.1. Preliminary Base Shear and Collapse Prevention Study

Figure (1b) portrays the responses of the constituent elements of the symbolic SDOF structure, where the P-delta moment is presented as the byproduct of an imaginary system with negative stiffness $K_{P\Delta}$. Note that in the design range limited by $\varphi_{max.}$ only the cantilever exhibits nonlinear behavior. Given W and $\Delta_e = \varphi_{max.} h_e$ the well-known relationship $T = 2\pi\sqrt{W / K_e g} = 2\pi\sqrt{\Delta_e / g}$, gives the secant stiffness $K_e = \Delta_e / W$, shown in Figure (1c), and the corresponding base shear as $V = K_e \Delta_e$. The external moment acting on the system can be shown to be equal to;

$$M = Vh_e + P\Delta_e = (V_F^P + V_C^E)h_e + P\Delta_e \quad (1)$$

where V_F^P and V_C^E stand for the plastic load capacity of the cantilever and the elastic shear carried by the truss/cable system, respectively. The total internal moment of resistance M_R, needed to prevent collapse can be estimated as:

$$M_R = \bar{M}_F^P + M_C^E = \bar{M}^P + (T_0 + T)\frac{dh_e}{l} = \bar{M}^P + M_0 + M_C \quad (2)$$

where T_0 and T are the initial and earthquake-induced tensile forces in the windward cable, respectively. Naturally, physical collapse can be prevented if $M_R > M$. Similarly, the necessary condition for possible recentering can be expressed as $V_C^E h_e > \bar{M}_F^P + P\Delta_e$.

2.2. Case 1-Full Cycle Analysis Leading to SSD

The purpose of case 1 is to illustrate how structural degradation can provide feedback on collapse prevention as well as PERR. Any ERS designed for SS, such as the symbolic structure of Figure (2a) and the proposed archetype of Figure (3), is expected to encounter four distinct stages of structural actions. The four-stage responses of the subject system are illustrated in Figures (2a) to (2f), where subscripts *E*, *V*, and *U* stand for elastic, first yield, and ultimate states, respectively. Ordinarily, a simple elastic analysis based on a prescribed loading regimen would be sufficient to design the subject structure. The same is not valid for SSD. In SSD, the loading process leading to incipient failure is followed by controlled unloading and reverse loading until PERR is achieved. The load-displacement relationships associated with the four operational stages can be

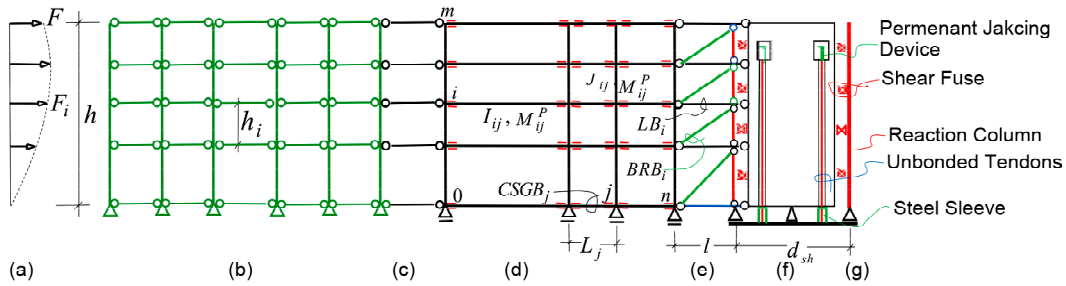

Figure 3. (a) Generalised lateral loading, (b) Articulated gravity structure, (c) Axially rigid links, (d) MF with REDMCs and grade beams, (e) BRBs+ links, (f) RRC+ stressed tendons and steel sleeves, and (g) Vertical supports for energy dissipating shear links (Not to scale).

expressed as follows:

1. The elastic response range; $V \le V_Y$ and $\Delta_E \le \Delta_Y$ Figures (2a) and (2c). This stage corresponds to the elastic response of the system. The tensile force in the windward and leeward cables is increased and decreased by an equal amount, respectively;
2. The elastoplastic response range; $V = V_Y$ and $\Delta_Y \le \Delta_P \le \Delta_U$, Figures (2c) and (2d). The replaceable column joint fails and sustains large ductile deformation while the cables stabilize and hold the system together. Unloading begins at the end of this stage. Despite the formation of a plastic hinge near the cantilever base, the system is still stable. The plastic collapse has been physically prevented;
3. The unloading stage; $0 \le V \le V_U$ and $\Delta'_R \le \Delta \le \Delta_U$, Figures (2d) and (2e). The lateral load ceases to exist. Δ'_R is the residual displacement after unloading. Although $V = 0$ at this stage, the system sustains the maximum P-delta moment that hinders the realignment process, and;
4. The realignment and repair stage; $0 \le |V| \le |-V_P|$ and $0 < \Delta'_R \le \Delta_R$, Figures (2e) and (2f). The function of this stage is to return the system back to its original, undeformed position using the stored elastic energies, i.e., to reduce $\Delta = \Delta'_R$ to zero. To achieve realignment, the elastic tension generated within the cables should be sufficient to overcome the sum of the residual forces related to the plastic hinge of the column and the lateral force generated by the $P\Delta'_R$ moment. Alternatively, forced recentering can be avoided by resorting to GSR and RFA. GSR is a recently developed technique to ease recentering, i.e., reducing the rotational stiffness of the column to zero by removing the damaged flange plates. The optional turnbuckles can always be utilized to help recenter the system as needed.

Replacement of the flange plates removes the major sources of residual displacements and facilitates the PERR process by reducing the stiffness of the cantilever to that of a simply supported column. New flange plates are then installed to complete the PERR process, as shown in Figure (2f). In conclusion, failure studies can provide feedback on the structure's response and help devise practical methods of PERR. It has been demonstrated that resilient framing can be expected to remain stable after sustaining seismic damage, can be recentered without recourse to large restoring forces [28]. It can also be repaired in a cost-effective manner [29]. The uniquely defined variable φ governs the deformations of the components of the structure of Figure (1). Assuming that both cables remain elastic throughout the history of loading, unloading, and recentering of the structure and that the lateral stiffnesses of the column and each one of the stays can be symbolized as K_F and K_T respectively, then the lateral displacement Δ corresponding to all four stages, described above, can be expressed as:

$$\Delta = \frac{V}{[2K_T + \delta_F^P K_F] f_{cr}} = \frac{V}{K^* f_{cr}} \tag{3}$$

where $f_{cr} = [1 - P/(2K_T + \delta_F^P K_F)]$ is the stability quotient of the subject system. The Kronecker's delta signifies loss of stiffness of the column as it becomes incapacitated. $\delta_F^1 = 1$ for $M_{conn.} \le \bar{M}^P < M^P$ and $\delta_F^P = 0$ for $M_{conn.} \ge \bar{M}^P$, where $M_{conn.}$ is the bending moment acting at the joint. The algorithm described in this section is used to develop the sustainable seismic design of the proposed archetype shown in Figure (3).

3. Development of the SS Archetype

The primary purpose of the current exercise is to devise a SS archetype and its components that can be constructed out of conventional means and construction methods. In short, a building type that can remain stable after sustaining controlled modes of damage can be recentered with no need for large restoring forces and that it can be built and repaired cost-effectively. SS is achieved by looking at PERR as reverse loading cycle after initial unloading and also planning and the fulfillment of the following operational criteria:

1. Pre-designated damaged parts due to controlled failure modes can be repaired as intended;
2. The entire building can be designed to lend itself to GSR and RFA or similar operations;
3. The entire building can be equipped with built-in or external means of realignment;
4. The entire building, including non-structural items, can be designed either to remain elastic after an earthquake or can be articulated for recentering without residual effects;

5. The entire building can be designed to remain stable after the incapacitation of groups of auxiliary devices and formation of plastic hinge patterns within the ERS and during the PERR processes;
6. The ERS should be as cost-effective as possible to offset expenses related to PERR operations.

A study of these criteria has led to the development of the SS archetype of Figure (3). The conceptual rules, research findings, and detailing requirements needed to fulfill the stipulated criteria are briefly discussed following the present section. The difference between a conventional system and SS archetype is the PERR process, which relies on CP and realignment methods.

The use of replaceable earthquake resisting devices can be effective if the structure is free from unaccounted stiffnesses and residual effects and when it is designed to sustain limited damage and is capable of being realigned after major earthquakes, otherwise no meaningful repairs can be achieved. Maintaining a large restoring/resisting force within the system is neither practical nor desirable. While the zero restoring force option looks attractive, it is impractical for conventional structural systems. Logistics aside, it is extremely challenging to stabilize a highly energized building at the brink of failure due to wind, deterioration, aftershocks, P-delta moments, etc. There are several reasons why it is not desirable to maintain a large restoring/resisting force within a single or limited number of elements. These include but may not be limited to:

- The safe planning of the recentering operations that rely on large pre-stressing forces. The elastic resistance of non-yielded components is of paramount importance, in that uncontrolled release of internal energies could trigger impact forces with extremely harmful effects;
- The use of additional elements and materials to resist compressive forces generated by the stressing system;
- Imbalanced loss of pre-loading within a single element, e.g., the RRC and/or the MF, can result in unforeseen displacements, P-delta effects, and a reduction in the global resistance of the structure;
- Unplanned, complete, or partial loss of the restoring/resisting forces could jeopardize, even thwart the PERR processes;
- The replacement of concentrated high energy sources, such as the post-tensioned cables, due to snapping may pose unforeseen challenges before, during, and after an earthquake.

In order to defuse or reduce the harmful effects of large restoring energies within a single element, the authors propose moderate pre-loading of as many independent members, such as link beams (LB), Figure (3c), SFs, Figure (3g), BRBs, Figure (3e) and earthquake resisting beams, Figure (3d). Furthermore, to control and achieve CP and PERR as efficiently as possible, the authors also propose the orderly use of GSR techniques combined with RFA. Two types of recentering strategies and their combinations can be utilized for PERR purposes. First is known as Forced Recentering, where the initial restoring moment is larger than the global moment of resistance of the ERS. The second is Assisted Recentering, where the magnitude of the initial restoring moment can be reduced to acceptable limits of pre-planned GSR and RFA. The controlled removal of REDMCs achieves GSR (see Figure 4). Here, the PERR process is looked upon as a controlled static process. The essence of the proposed methodology is the revelation that the stiffness of

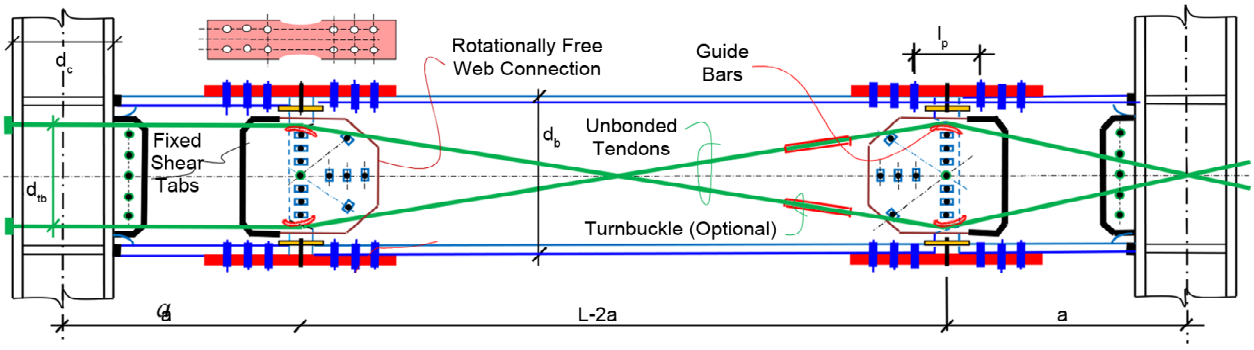

Figure 4. Self-aligning REDMC arrangement with optional post-earthquake realignment X tendons fixed at one end and continuous at the other.

the proposed archetype with replaceable, controlled strength parts, e.g., the articulated beam joints, is not a function of the strength of the system, while the same is not always valid for conventional systems without strength controlling devices.

3.1. Governing Rules and Research Findings

The rationale leading to the development of the proposed archetype of Figure (3) and the corresponding design methodologies is essentially based on the results of the following research findings:

- In SSD, the response of the structure to unloading and reverse loading is as important as its response to the loading stage;
- The residual moment formed at the end of the half-cycle of the normal hysteresis curve of a ductile system plus the corresponding P-delta moment may be interpreted as the magnitude of the minimum restoring force needed to realign the structure after the quake has subsided;
- As the global stiffness is directly related to the global strength of the MF and that the minimum recentering force is equal to or greater than the global strength, then the minimum restoring force at reduced stiffness should be equal to or greater than the corresponding reduced global strength;
- Ordinarily, the post-earthquake restoring moment, including the P-delta effect, needed for realignment is larger than the original seismic moment;
- The larger the capacity, the smaller the residual drift and the larger the restoring moment needed to realign the system;
- The P-delta effect tends to reduce the global stiffness of the structure during the loading phase and increase the same during the recentering process;
- If the global stiffness of the MF is reduced to zero by removing all replaceable fuses, including the damaged flange plates, after unloading, then no restoring moment other than that needed to counter the P-delta effect would be required to realign the system;
- The possibility to avoid damage to the body of the beams not only removes the major sources of residual deformations but also facilitates the PERR process by reducing the stiffness of the MF and or adjusting the restoring moment to that of a stable mechanism or residue-free frame;
- CP is achieved by preventing the activation of failure mechanisms rather than strengthening isolated members;
- Planned articulation is the key to the residue-free design and successful PERR;
- All replaceable parts, fuses, and articulated connections should be treated as protected zones;
- Rational damage analysis can lead to efficient, sustainable seismic design.

3.2. SSD and Material Optimization

SSD is generally related to incipient collapse at ultimate loading. Therefore, it seems rational to resort to pre and post-damage analysis of the earthquake-resisting MF of the prototype or the ERS with a view to materials and construction cost saving. The basic idea behind the proposed argument is that structural efficiency is mainly a function of system characteristics and modes of failure rather than numerical analysis and that seismic input energy, unlike gravity loading, is also a function of structural attributes and design. A structure may be efficient and workable, from an SS point of view, if its total weight and drift at maximum damage are minimum [30], and that damage can be limited to identical repairable parts with the least possible cost and effort. The purpose of this section is to describe the steps leading to the development of a highly efficient basic module that satisfies the pre and post-damage requirements of a workable, flexural SS module as presented in section 3.2.1 below.

Utilizing the SSD concept in the archetype of Figure (3) will force the MF to have a uniform drift along with the height. This will lead to a uniform strength demand on MF beams in all stories. The uniform section of beams, unique connection detail, simplicity of fabrication and installation, ease of work commencement provide other aspects of construction work optimization.

3.2.1. Pre-failure Conditions, Elastic State

Consider the responses of the basic modules of Figures (5a), (5b), and (5c), with generalized member strengths and stiffnesses, under identical loading conditions. Module (4a) is composed of four different members. Since V is reversible the two columns should be identical, as illustrated in

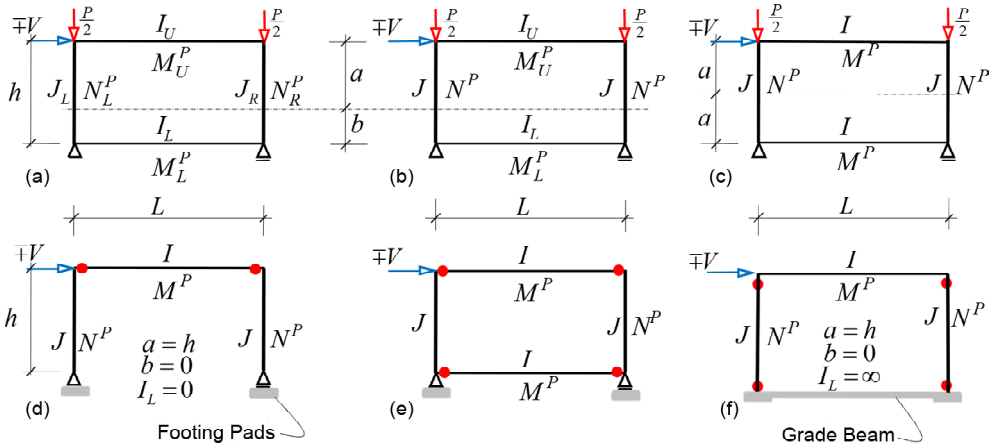

Figure 5. (a) Generalised basic module, (b) Module with identical columns, (c) Doubly symmetric module, (d) Pinned base module (e), Grade beam supported module, and (f) Fixed-base module.

Figure (5b), i.e., $J_L = J_R = J$, hence, the elastic drift ratio $\phi = \Delta / h$, of the basic module of Figure (5b), subjected to forces V and P, may be expressed as:

$$\phi = \frac{V}{12Ehf_{cr}}\left[\frac{2(a^3+b^3)}{J}+\left(\frac{a^2}{I_U}+\frac{b^2}{I_L}\right)L\right]=\frac{V}{hKf_{cr}} \tag{4}$$

where $f_{cr} = 1 - P / Kh$. J, I_L and I_U are the moments of inertias of the columns, the lower and the upper beams, respectively. Δ is the roof level displacement. Dimensions a and b describe the distances of the upper and lower beams of the module from the imaginary horizontal neutral axis of the frame. The condition for minimum drift with respect to the location of the neutral axis can be expressed as:

$$\frac{\partial\phi}{\partial a}=0 \quad \text{or} \quad \frac{\partial\phi}{\partial b}=0 \tag{5}$$

Introducing $\rho = (JL / I_U h)$ and $\bar{\rho} = (JL / I_L h)$, and performing the differentiation (5) gives;

$$\frac{a}{h}=\frac{3+\bar{\rho}}{6+\rho+\bar{\rho}}, \quad \frac{b}{h}=\frac{3+\rho}{6+\rho+\bar{\rho}}$$

and

$$\frac{a}{b}=\frac{3+\bar{\rho}}{3+\rho} \tag{6}$$

Let $S = 3 + \rho$ and $\bar{S} = 3 + \bar{\rho}$ define the upper and lower racking stiffnesses of the basic frame, respectively. Then the corresponding upper and lower beam end moments M_U and M_L can be expressed as:

$$M_U = \frac{Va}{2f_{cr}} = \left(\frac{Vh}{2f_{cr}}\right)\frac{S}{S+\bar{S}} \tag{7a}$$

$$M_L = \frac{Va}{2f_{cr}} = \left(\frac{Vh}{2f_{cr}}\right)\frac{\bar{S}}{S+\bar{S}} \tag{7b}$$

A simple check verifies that the sum of the beam end moments is equal to the total racking moment $M_{Rack.}$ i.e.,

$$M_{Rack.} = 2M_U + 2M_L = 2\left[\frac{Va}{2f_{cr}}+\frac{Vb}{2f_{cr}}\right]=\frac{Vh}{f_{cr}} \tag{8}$$

The suitability of ERS in general and MFs, in particular, is basically a function of their boundary support restraints during all loading conditions. The versatility of Equation (4) allows the attributes of pinned, fixed, and grade beam supported modules to be compared in terms of their structural responses, economics, and possibilities of PERR. Substitution of the pertinent sets of characteristic parameters, $(a = h,\ b = 0,\ I_L = 0)$ $(a = b = h/2, I_U = I_L = I, J_L = J_R = J)$ and $(a = h, b = 0, I_U = I, I_L = \infty, J_L = J_R = J)$, in Equation (4) results in the elastic load-deformation relationships of the basic modules of Figures (5d), (5e), and (5f) respectively, i.e.

$$\begin{aligned}\phi_{pin} &= \frac{Vh}{12Ef_{cr,pin}}(2\rho+1)\\ \phi_{grd} &= \frac{Vh}{24Ef_{cr,grd}}(\rho+1)\\ \phi_{fix} &= \frac{Vh}{12Ef_{cr,fix}}\left(\frac{3+2\rho}{6+\rho}\right)\end{aligned} \tag{9}$$

It follows that $\phi_{fix} < \phi_{grd} < \phi_{pin}$. Apparently selection of the fixed boundary supports appears most suitable for the purpose. However, material consumption, constructability, and, most importantly, reparability conditions should also be studied before making a final decision. The moment-deformation relationships of the beams of module (5b), in terms of upper and lower beam end rotations θ_U and θ_L, can be expressed as $M_U = 6EI_U\theta_U / L$ and $M_L = 6EI_L\theta_L / L$ respectively. Assuming that $M_U > M_L$ and that the column design moment $N = M_U$, then the module linearized non-plastic total weight function may be computed as $G = \gamma \times [LM_L + (2h + L)M_U]$, where γ is an arbitrary constant of proportionality. Substituting for M_L from Equation (7) into the weight equation and rearranging, it gives:

$$G = \gamma\left[2hM_U + \frac{VhL}{2f_{cr}}\right] = \gamma\left[12EI\theta + \frac{VhL}{2f_{cr}}\right] \tag{10}$$

Now since by assumption $M_U > M_L$ then for a non-zero solution, Equation (10) may be studied in conjunction with the following limiting conditions;

$$\frac{Vh}{4f_{cr}} \geq \left[M_L = \frac{6EI_L\theta_L}{L}\right] > 0 \quad \text{and}$$
$$\frac{Vh}{2f_{cr}} \geq \left[M_U = \frac{6EI_U\theta_U}{L}\right] > \frac{Vh}{4f_{cr}} \tag{11}$$

Comparing inequalities (11) with Equation (10), it follows that the total weight of the module is minimum when $M_U = M_L = Vh / 4f_{cr}$ and / or $I_U\theta_U = I_L\theta_L$, which can be true only when $I_U = I_L = I$ and $\theta_U = \theta_L = \theta$, i.e., when $a = b = h/2$. In other words, the doubly symmetric module of Figure (5c) represents the most efficient solution, where both the total weight and side-sway are minimum, i.e., the demand-based non-plastic total weight and the corresponding drift ratio become:

$$G = 2\gamma(h + L)M_U \quad \text{and} \quad \phi \text{ from Eq. 8} \tag{12}$$

Equation (12) leads to the simple but important conclusion that; the most efficient design of the grade beam supported module is one that involves double symmetry as opposed to single or non-symmetric configurations. The results of this finding are extended to the design of modules of multimember earthquake resisting MFs of section 6, Figure (6).

3.2.2. Post-Failure Conditions, Plastic State

Figures (5d), (5e), and (5f) portray the plastic hinge patterns of the same portal frame, with different boundary conditions associated with purely sway type failure mechanisms due to lateral loading. The plastic carrying capacities of the three cases can be summarized as follows:

$$M^P_{pin} = \frac{Vh}{2f_{cr,pin}}, \quad M^P_{grd} = \frac{Vh}{4f_{cr,grd}} \quad \text{and}$$
$$M^P_{fix} = \frac{Vh}{4f_{cr,fix}} \tag{13}$$

Assuming the weight value of the concrete grade beam of Figure (5f) is practically the same as that of the lower beam of Figure (5e), then the capacity based total weight of the three cases can be expressed as:

$$G_{pin} = \gamma(L + 2h)M^P_{pin} = \frac{\gamma(L + 2h)Vh}{2f_{cr,pin}},$$
$$G_{grd} = 2\gamma(L + h)M^P_{grd} = \frac{\gamma(L + h)Vh}{2f_{cr,grd}} \quad \text{and} \tag{14}$$
$$G_{fix} = 2\gamma(L + h)M^P_{fix} = \frac{\gamma(L + h)Vh}{2f_{cr,fix}}$$

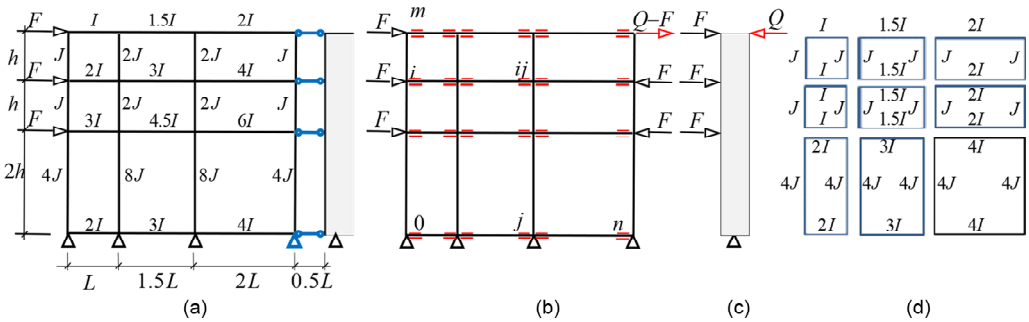

Figure 6. (a) RC-MFUS, (b) MF free body diagram, (c) RRC free body diagram, and (d) Imaginary modules.

Since $G_{fix} < G_{grd} < G_{pin}$ and $\phi_{fix} < \phi_{grd} < \phi_{pin}$, according to Equation (8), then selection of fixed boundary supports appears more advantageous than the other two options. Although fixed base modules sustain the least possible drift due to lateral loading, they are prone to the formation of plastic hinges at column supports and or within the footings, as shown in Figure (5f). Multistory columns with damaged supports and any degree of residual drift are extremely difficult to repair or replace. Reparability is the single most important factor in SSD. Therefore, the best workable choice is the doubly symmetric module of Figure (5c). Furthermore, doubly symmetric modules lend themselves better to uniform distributions of plastic hinges and disposition of inflection points at mid spans of all beams and columns. For this reason, only the possibilities of grade beam supported modules are studied in the rest of this paper.

The high rigidity of the rocking core forces the entire building to act as an SDOF system and causes all other components to absorb proportional amounts of energies [26]. And, if this is the case, the moment-drift relationship of the entire MF can be expressed as [31]:

$$\phi = \frac{(M_F + M_{P\Delta})}{12E} \times \left[\frac{1}{\sum_{j=0}^{n} \sum_{i=1}^{m} \bar{\delta}_{i,j}^{P} \bar{k}_{i,j}} + \frac{1}{\sum_{j=1}^{n} \sum_{i=0}^{m} \delta_{i,j}^{P} k_{i,j}} \right] = \frac{M_F}{K_F f_{cr}} \quad (15)$$

For a description of $\delta_{i,j}^{P}$ and $\bar{\delta}_{i,j}^{P}$ the interested reader is referred to Appendix A and case 3.

4. Design of the Essential Components

Ideal SS cannot be realized unless every part of the system is designed to remain practically residue-free and/or repairable after earthquakes.

In the contexts of SS and PERR, special detailing is referred to elements and connections that are supposed neither to dissipate seismic energy nor hinder the realignment process due to accumulation of residual stresses and strains, e.g., non-bearing walls and infills constructed within the bays of MFs and theoretically moment free column supports. To alleviate such problems and increase reparability, special items should be designed in such a way as to remain practically articulated at all times or to be capable of becoming articulated and/or removable before recentering. For successful planning of the proposed archetype, the following detailing issues have been addressed in some detail.

4.1. The Gravity Structure

The large-displacement interactions of the gravity structure with the earthquake resisting and realigning systems are practically never considered. Damage sustained by the gravity and non-structural elements can be as harmful as those of the earthquake-resisting members. In almost all conventional frameworks, the gravity system tends to resist earthquake forces in proportion to its neglected stiffnesses and hinders the recentering process due to earthquake-induced residual effects. Richards et al. [32] and Astaneh-Asl et al. [33] have shown that significant moments can develop when specific bolt patterns and sizes and plate thicknesses are used for simple connections. Therefore, it is imperative to design the elements of the gravity systems envisaged for SS in such a way as to be free from seismic forces and not to endure residual strains (generic solutions to such issues can also be found in reference [8]). Unwarranted deformations of the gravity system can be avoided or at least minimized if pinned base columns and articulated beam-column joints such as those shown in Figure (7b), as opposed to standard beam-column connections, Figure (7a), are used for the purpose. The web plates are detailed with elongated holes that avoid earthquake-related residual strains at both ends of simply supported beams. All such details should be regarded as protected zones requirements.

4.2. Column Supports and Footings

Although many frame structures designed following the weak-beam/strong-column concept have survived earthquakes without catastrophic collapse, the cost of repairing the many locations of inelastic damage, especially at the fixed base of wall and column supports, has often been excessive [34]. Formation of plastic hinges at column feet increases drift concentration and works against smooth recentering. The drawbacks of fixed base boundary conditions for MFs can be alleviated by introducing column support grade beams (CSGB), as shown in Figure (3d). Pairs of

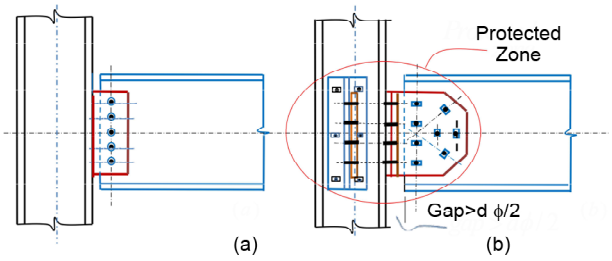

Figure 7. (a) Standard simple beam-column connection, (b) Articulated simple residue-free (no bending, no torsion beam connection, d: beam depth).

REDMCs at the ends of the grade beams prevent damage to the footings, base plates, and the formation of plastic hinges at column supports. The rotational controllability of the column supports prevents damage to the footings, facilitates the PERR process, and helps maintain uniform drift along the structure's height. This, in turn, helps the structure respond as an MF of uniform shear (MFUS) [35]. The strength, stiffness, and other properties of the footings and the supporting medium are selected in such a way as to prevent relative settlements of all vertical elements such as rocking walls, columns, stabilizing tendons, energy dissipating devices, etc.

4.3. The Butterfly Steel Shear Fuses

The parallel tilting of the RRCs and adjoining columns, Figures (3f) and (3g), provides opportunities for making use of replaceable butterfly type SFs or similar devices. There is sufficient evidence that properly designed SFs can improve overall damping, reduce seismic demand on ERS and prevent collapse. Figures (8a) and (8b) depict generic arrangements of energy dissipating steel shear plates with regular openings, bolted or welded to relatively rigid parallel supports. The welded version is less prone to lateral-torsional buckling, but the bolted type is easier to install and repair. Steel plate SFs are generally provided with horizontal slots and stiffeners for easy yielding and out-of-plane stability. A helpful analysis and design guide for butterfly fuses has been compiled by [36]. The force-deformation relationship of symmetrically disposed lines of SFs can be expressed as;

$$\phi = \frac{M_S}{K_S} \tag{16}$$

where $K_S = m.d_{sh}.F_{sf}$, in which F_{sf} is the total carrying capacity of SFs for each supporting column and d_{sh} is the horizontal distance between the two columns, Figure (8b).

4.4. Buckling Restrained Brace (BRB) and RRC Interaction

BRBs are commercially available and specially designed members that can withstand relatively large axial strains without buckling and usually are used as parts of earthquake-resistant braced frames, Figure (3e). All members of the braced frame are treated as pin-ended elements. The two verticals are continuous, relatively rigid, steel pin-supported columns. Here, BRBs have been utilized as supplemental devices for reducing seismic demand on the system, increasing overall damping, and possibly preventing plastic collapse. However, due to low post-yield stiffness, they cannot be relied upon as primary recentering elements. On the other hand, most BRBs exhibit sufficiently stable hysteretic behavior and can be easily installed and removed as needed. Because of such attributes, BRBs can be utilized effectively in conjunction with GSR and RFA operations. The force-deformation relationship of the braced frame of uniform response of

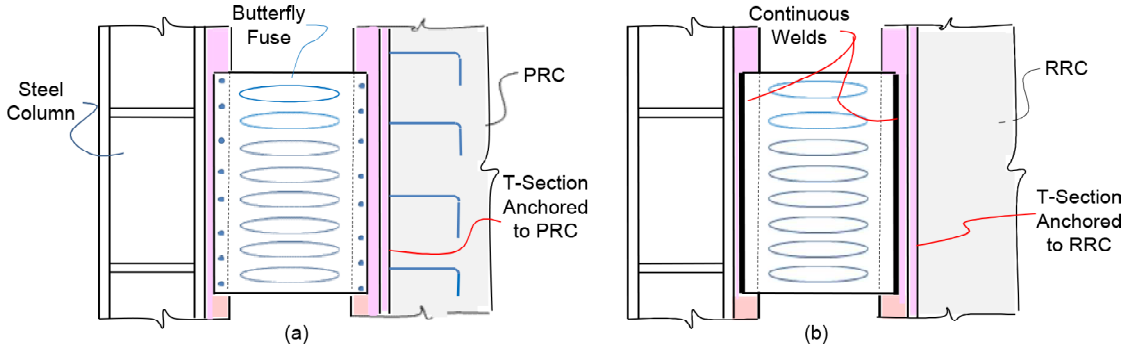

Figure 8. Generic replaceable shear fuses, (a) Bolted to continuous side plates/steel sections and (b) Welded to continuous side plates/steel sections (not all details shown for clarity) .

Figure (3e) can be expressed as:

$$\phi = \frac{M_B}{l^2 E_B \sum_{i=1}^{m} (h_i^2 A_i / \bar{L}_i^3)} = \frac{M_B}{K_B} \qquad (17)$$

where $\bar{L}_i$ and A_i stand for length and effective cross-sectional area of the BRB at level i, respectively.

4.5. The Link Beams

The function of the link beams (LB), Figures (3c) and (3e) is twofold, first to transmit the seismic forces generated within the system to the RRC and redistributing restoring forces from the RRC to the entire structure, and if required, to generate restoring moments at one or both ends. Therefore, all LBs should be designed as axial elements that remain elastic and stable during both the seismic event as well as the PERR operations. However, if the beams of the MF are equipped with gap opening continuous post-tensioned tendons, as in Figures (4) and (9), then it would be logical to pass the same set of tendons through the LBs with similar gap opening profiles as for the beams and extend the tendons into the RRC for anchorage. The single or double shear tabs at both ends are detailed with radially arranged elongated holes that avoid earthquake-related residual strains. Both ends of the LBs are specified as protected zones.

4.6. The Rocking Core

Fixed base reinforced concrete shear walls are practically difficult to repair after severe cracking and formation of plastic hinges at the lowermost regions of the wall and restrict the controllability of the entire structure. The most common drawbacks associated with fixed base shear walls can be alleviated by introducing centrally articulated hinge support as shown in Figure (3f).

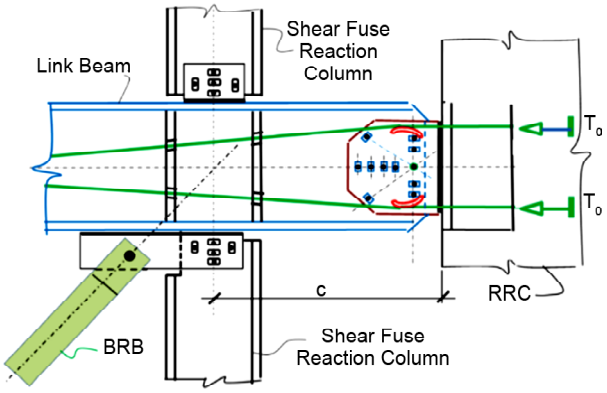

Figure 9. Steel link beam supporting reaction column and BRB.

Figure (10) illustrates two controllable elastoplastic base arrangements with extensive displacement capabilities in which the axial and shear forces are decoupled and sustained independently by partially sleeved tendons or direct energy absorbing elements and the central hinge systems, respectively. The RRC sometimes referred to as building strong spine, is the most important feature of the proposed archetype. Depending on the type of construction, material availability, or regional engineering practice, RRCs can be constructed using wooden panels, steel shear walls, post-tensioned reinforced

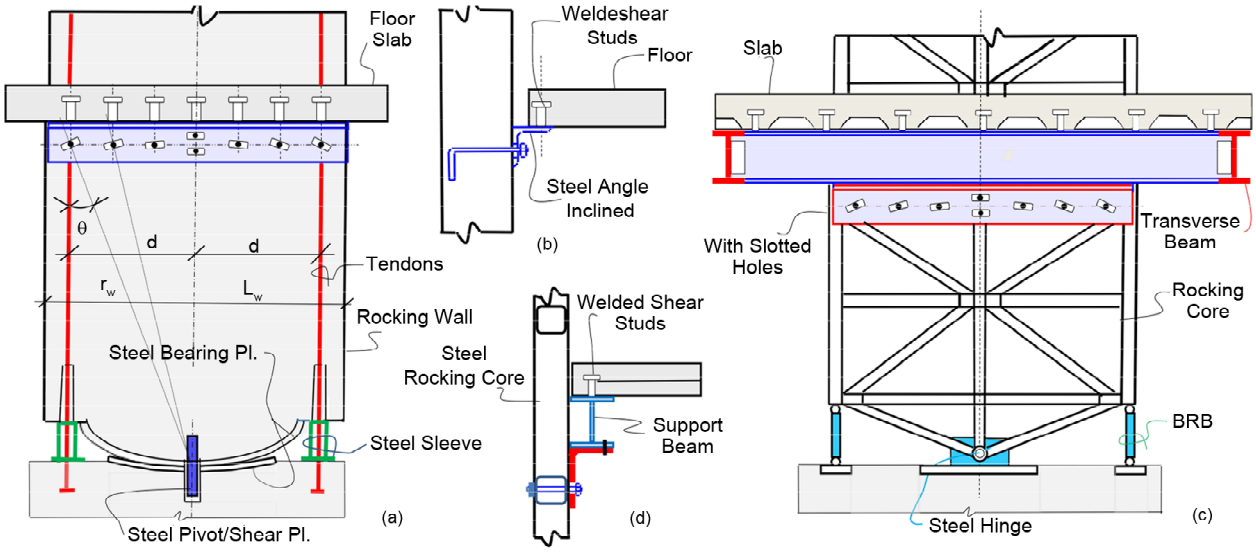

Figure 10. (a) Generic concrete RRC, diaphragm and base level connections (b) Side view of (a), (c) Generic BRB enhanced Steel RRC, diaphragm, and base level connections, and (d) Side view of (c).

concrete, or steel braced frames [37]. Diaphragm inertia forces are transferred to the RRC through un-bonded PT strands, Rigid Link Beams (LBs), Buckling Re-strained Braces (BRBs), and shear connectors between the floors slab and the RRC. Restoring properties of RRCs are defined by their base-level rotational stiffness, system rigidity, and ultimate strength. For a complete list of the important attributes of RRCs, the interested reader is referred to [19]. The rocking motion of the RRC tends to induce vertical and horizontal forces along its interfaces with the shear columns, floor, and roof level diaphragms. Almost the entire tributary seismic force is transmitted to the RRC through the LBs. While the horizontal components of the rocking movement tend to slide the core against the floor and roof diaphragms, the vertical components tend to twist and damage the connected slab/diaphragm regions along the interface. The problem is resolved by providing strategically located elongated bolt holes perpendicular to their radii of rotation along each interface, Figures (10a) and (10c). The physical clearances between the slabs and the RRCs prevent the core-slab connections from being damaged during earthquake-induced lateral displacements. Radially inclined elongated holes allow free movement of the core and provide out-of-plane stability for the RRC. Figure (10a) also shows the location of the center of the most critical hole at the left hand end of the connecting angle with respect to the center of rotation of the RRC by radius r_w and radial inclination θ. However, if ϕ is small, the vertical and horizontal components of the radial displacement of the bolt center can be computed as $\pm\phi d \sin\theta$ and $\pm\phi r_w \cos\theta$ respectively. This implies that a combination of oversized wide slotted holes, in lieu of inclined slotted holes, may be tolerated for most cases. The moment-rotation relationship of the RRC as derived in section 5 is;

$$\phi = \frac{M_C}{K_C} \tag{18}$$

4.7. Non-Structural Components

Partition walls, infills, facades, stairways, escalators, non-structural utility shafts, lifelines, ductworks, mechanical equipment, suspended ceilings, and similar items should be secured in place in such a way as not to contribute to seismic resistance nor hinder the realignment process. This would also prevent seismic damage to all such items. Figure (11) depicts a number of combinations of structural and non-structural infills and MFs that can cause seismic damage and impede the recentering effort. It also illustrates some simple details for MF-infill combinations, where wall and column damage is prevented, and recentering can occur without obstructive conditions. Figure (11a) represents a solid infill that is capable of withstanding seismic and gravity forces at the same time.

However, if the columns are not detailed as boundary elements and securely tied to the infill, then a short column condition with the formation of unforeseen plastic hinges within the columns may occur. Figure (11b) depicts a similar loading state with the difference that the gaps between the columns and the infill allow free movements of the columns without contact with the infill. The short column phenomenon is avoided. Figures (11c) and (11d) illustrate the same configurations under pure gravity and pure shear conditions, respectively. The horizontal gap between the top of the infill and the soffit of the steel beam of case (11d) avoids the transmission of axial forces to the infill. The welded steel plates on either side of the infill with horizontal and vertical slotted holes help release the undesired restraint in each case. Figure (11e) with gaps on three sides shows a freestanding infill supported in such a way as not to fail due to out of

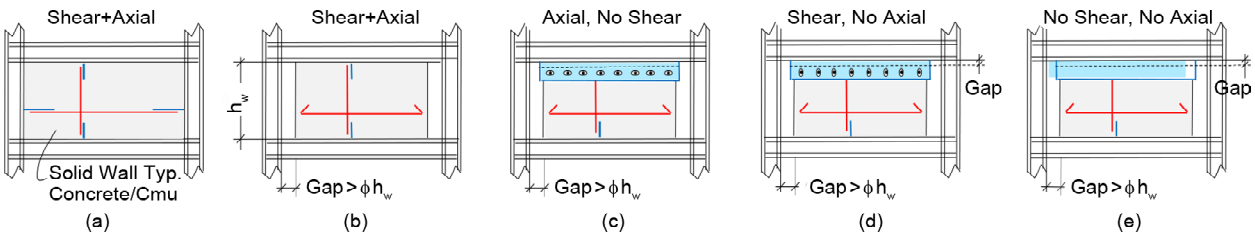

Figure 11. (a) Shear + axial wall with column as boundary element, (b) Detached Shear+axial (c) Axial bearing with no shear, (d) Shear transfer no axial bearing, and (e) Freestanding solid partition (not to scale).

plane forces. Another area of seemingly trivial concern is the behavior of end restrained stringers of concrete and steel stairs that act as heavy braces connecting consecutive floors to each other. The authors believe that releasing the horizontal restraints at the lower end of the stringers may alleviate the uncontrolled interactions between consecutive floors. Although such details may seem trivial and straightforward, their correct or wrong implementation may mean the difference between success and failure, respectively.

4.8. Sequential Response of the Earthquake Resisting Systems

Since all structures of the proposed archetype are connected in parallel, then their combined resistance against the external moment $(M + M_{P\Delta})$ can be expressed as:

$$(M + M_{P\Delta}) = M_F + M_S + M_B + M_C + M_M \qquad (19)$$

subscripts *F*, *S*, *B*, *C*, and *M* refer to frame, shear fuse, brace, core, and miscellaneous, respectively. Substituting for etc., from Equations (15) through (19), gives after simplifications;

$$\phi = \frac{(M + M_{P\Delta})}{(\delta_F^P K_F + \delta_S^P K_S + \delta_B^P K_B + \delta_C^P K_C + \delta_M^P K_M)} = \frac{M}{\bar{K} f_{cr}} \qquad (20)$$

where $\delta_{Item}^{Plastic}$ has the same meaning as defined under section 1.2 above. $\delta_{Item}^{Plastic} = 1,$ or zero is a function of the rule of sequential failures which states that:

$$\frac{M_a^P}{K_a} < \frac{M_b^P}{K_b} < \frac{M_c^P}{K_c}, \ldots < \frac{M_d^P}{K_n} \qquad (21)$$

Equation (21) implies, if all systems act together, the first and last stage failures will occur at $\phi_a^P = M_a^P / K_a$ and $\phi_n^P = M_n^P / K_n$ where ϕ_a^P and ϕ_n^P maybe looked upon as the initial and smallest, and the last and largest deformation of the loading history of the combined system.

5. Development of Controllable Gap Opening Segments

Unrestricted gap opening segments were originally devised to improve the seismic performance of certain types of ERS, such as special MFs and eccentrically braced frames [38]. Here, the use of the gap opening concept has been modified to controllable PERR and enhances the overall seismic performance of the system. The use of controllable gap movement increases the capacity of the joint and helps implement GSR and RFA procedures. The main drawback of pre-loaded cables is their vulnerability to premature yielding, relaxation, and decompression due to overloading. Most of these issues can be resolved through purpose-specific detailing and the provision of grade level steel sleeves. Recentering by means of GSR becomes even more attractive when utilized in conjunction with RFA techniques, i.e., using reliable, self-activating, or manually controlled equipment. Many options are available. As engineers become acquainted with RRCs and their applications, so grow the concerns and queries regarding their maintenance, repairs, and controllability after prolonged periods of inactivity, major earthquakes, and subsequent aftershocks. Some of the more important issues, regarding these concerns, can be summarized but may not be limited to the following:

- Accidental or underestimated slacking or decompression of the leeward tendons that may lead to diminished core strength, stiffness and stability;
- Yielding of the windward or front tendons due to overloading, material flaws, etc. that could lead to similar effects caused by the slacking of the leeward tendons;
- Protection of the free lengths of the tendons along the open gaps against fire, corrosion, clogging, etc., that may endanger the stability of the RRC and hinder the PERR operations;
- Initial imperfections of RRC, e.g., uncontrolled leaning of RRC towards or away from the main structure, during and after construction;
- The need for manual or automated tensioning/de-tensioning of the tendons for adjustments or as needed for PERR;
- The need for a fail-safe system to assure static stability of the freestanding RRC in the absence of the tendons;
- The need to adjust the initial resistance of the RRC for design and or rehabilitation purposes;
- The need to adjust the initial resistance of the RRC due to such losses as creep, shrinkage,

relaxation, etc.

The performance of the RRC can be enhanced by equipping it with cost-efficient secondary systems that ensure continued operation if the primary system fails. In practical terms, this implies the implementation of the following ideas:

1. Provision of permanent, ready-to-operate stressing jacks placed in accessible locations within the core, such as Figures (3f) and (12a). The size and capacity of the stressing devices will depend upon the force and nature of the tendons specified for the project.
2. Provision of devices and or details that would compensate for diminished performance of RRC due to decompression of the leeward tendons.
3. Addition of protective, load-bearing steel sleeves (round pipes or square tubes) that cover the unprotected lengths of the stressed tendons along the open gap and provide supports for the core in the absence of stabilizing tendons. A symbolic depiction of the proposed sleeves is presented in Figures (10a) and (12a).

The characteristics of the sleeves are dictated by their dual functions as secondary supports for the core as well as compensating devices for the slacking of the de-tensioned tendons. The sleeves are anchored to non-yielding supports at their lower ends and hinged to the lower ends of the core. The sleeves are capable of absorbing the overturning forces generated by the RRC and the out-of-balance forces of the core. The sleeves are tension/compression elements that are designed to remain elastic without buckling. The tendon-sleeve combination acts as a pseudo tension/compression member. Assuming the axial stiffness of the sleeves is negligible compared with that of the core, the axial deformations of the tendons and the sleeves due to initial tensioning T_0 can be computed as:

$$\varepsilon_t = \frac{T_0 h}{A_t E_t} = \frac{T_0}{k_t} \quad \text{and} \quad \varepsilon_s = 0 \tag{22}$$

where by definition k_t and $k_s = A_s E_s / h_s$ stand for axial stiffnesses of the tendons and the sleeves, respectively. Subscripts t and s refer to tendons and sleeves, respectively.

5.1. Response Condition 1

Before lateral loading $T_{L,t} = T_{R,t} = -T_0$, $C_{L,s} = C_{R,s} = 0$ and $R_0 = 2T_0$, Figure (12a). Subscripts L and R refer to left and right-hand sides, respectively. Upon lateral loading, the clockwise overturning moment Fh of Figure (12b) tends to lift up and push down the left and right-hand sleeves, respectively. Since the RRC is extremely rigid, both tendons and sleeves elongate and shorten equally, i.e.,

$$\left|\varepsilon_{L,t}\right| = \left|\varepsilon_{L,s}\right| = \left|\varepsilon_{R,t}\right| = \left|\varepsilon_{R,s}\right|$$

or

$$\left|\partial T_{L,t} / k_t\right| = \left|\partial C_{L,s} / k_s\right| = \left|\partial T_{R,t} / k_t\right| = \left|\partial C_{R,s} / k_s\right|$$

This gives,

$$\partial C_{L,s} = -\partial C_{R,s} = (k_s / k_t)\partial T_{L,t}$$
$$\partial T_{R,s} = -\partial T_{L,t}$$
$$\partial R_L = \partial T_{L,t} + \partial C_{L,s}$$
$$\partial R_R = \partial T_{R,t} + \partial C_{R,s}$$

Static equilibrium requires that,

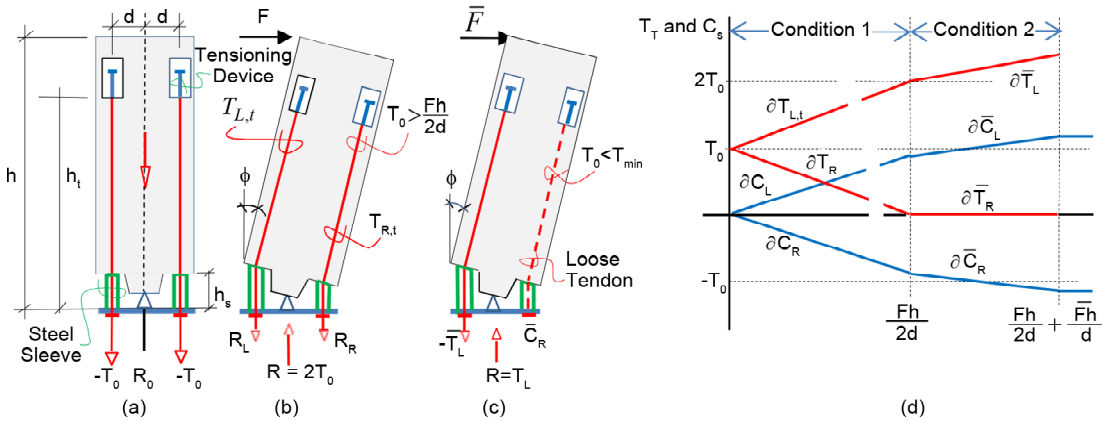

Figure 12. (a) Pre-loaded RRC with un-bonded PT tendons and compressible sleeves, (b) Condition 1: both tendon in tension (c) Condition 2: leeward tendon slackened, and (d) Variations of T(tension) and C (compression) with core force RRC.

$Fh = (R_L + R_R)d =$
$(T_0 + \partial T_{L,t} + \partial C_{L,s} - T_0 + \partial T_{R,t} + \partial C_{R,s})d =$
$2[1 + (k_s / k_t)]\partial T_{L,t} d.$

It follows that in the range $T_0 > \partial T_{R,t} > 0$ where $T_{R,t}$ is still in tension, $\partial T_{L,t} = [k_t / (k_t + k_s)] \times (Fh / 2d)$, $\partial T_{R,t} = [k_t / (k_t + k_s)](Fh / 2d)$, $\partial C_{L,s} = [k_s / (k_t + k_s)](Fh / 2d)$ (tens.), $\partial C_{R,s} = [k_s / (k_t + k_s)] \times (Fh / 2d)$ (comp.) and $\partial R = \partial R_L - \partial R_R = 0.$ Consequently the total tendon forces become $T_{L,t} = T_0 + [k_t / (k_t + k_s)]Fh / 2d$ (tens.) and $T_{R,t} = T_0 - [k_t / (k_t + k_s)]Fh / 2d$ (tens.), and total sleeve forces become $C_{L,s} = \partial C_{L,s} = [k_s / (k_t + k_s)](Fh / 2d)$ (tens.) and $C_{R,s} = \partial C_{R,s} = [k_s / (k_t + k_s)](Fh / 2d)$ (comp.). At the end of condition 1, the right-hand tendon slackens whence $T_{R,t} = (T_0 - \partial T_{R,t}) \to 0$, i.e., $\partial T_{R,t} \to T_0$. This leads to $T_{L,t} = (T_0 + \partial T_{L,t}) = 2T_0$ (tens.), $C_{L,s} = \partial C_{L,s} = [k_s / (k_t + k_s)](Fh / 2d)$ (tens.), $C_{R,s} = \partial C_{R,s} = [k_s / (k_t + k_s)](Fh / 2d)$ (comp.) $R \to (R_0 + \partial R) = 2T_0$.

Note that in this range, the pair of sleeves resist a maximum overturning moment equal to $M_R = 2(T_0 + C_{R,s})d = Fh$ until the leeward tendon becomes loose. Also, note that because of symmetry T_0 does not enhance the potential restoring moment but tends to increase the stiffness of the cable system. Following Equation (22), deformations of the core can be computed as $\varepsilon_t = \varepsilon_s = \partial T_{L,t} / k_t$, and the corresponding rotation of the core can be estimated as:

$$\phi = \frac{\varepsilon_s}{d} = \frac{\partial C_{R,s}}{k_s d} = \frac{M_C}{2(k_s + k_t)d^2} = \frac{M_C}{K_C} \tag{23}$$

5.2. Response Condition 2

The initial condition of this phase is characterized by the end conditions of response condition 1, Figure (12c). Static equilibrium for this stage requires $\bar{F}h = (\bar{T}_L + \bar{T}_R)d = (\partial T_{L,t} + 2\partial C_{L,s})d = [1 + (2k_s / k_t)]\partial T_{L,t} d$, or $\partial \bar{T}_{L,t} = [k_t / (k_t + 2k_s)] / \bar{F}h / d$ (tens.) and $\partial \bar{C}_{L,s} = [k_s / (k_t + 2k_s)] / \bar{F}h / d$ (tens.) and $\partial \bar{C}_{R,s} = [k_s / (k_t + 2k_s)] / \bar{F}h / d$ (comp.). Upon additional loading, the internal forces of the left-hand side tendon and sleeve increase from $2T_0$ to $2T_0 + \partial \bar{T}_{R,t}$ (tens.) and from $C_{L,s}$ to $C_{L,s} + \partial \bar{C}_{L,s}$ (comp.), respectively. Similarly, the internal force of the right-hand sleeve increases from $C_{R,s}$ to $C_{R,s} + \partial \bar{C}_{R,s}$ (comp.) while the corresponding tendon force remains zero $\bar{T}_{R,t} = 0$. Here the bar over a symbol relates it to response condition 2. The core's left, center, and right-hand reactions (condition 2 loading) become $\bar{T}_L = 2T_0 + \partial \bar{T}_{L,t} + C_{L,s} + \partial \bar{C}_{L,s}$, $R + \bar{R} = 2T_0 + \partial \bar{T}_{L,t}$, and $\bar{C}_R = C_{R,s} + \partial \bar{C}_{R,s}$ respectively. Unlike condition 1, the magnitudes of the total moment of resistance of condition 2 are influenced by $T_0 + \partial T_{R,t}$, i.e., $M + \bar{M} = (2T_0 + C_{L,s} + C_{R,s} + \partial \bar{T}_{L,t} + \partial \bar{C}_{L,s} + \partial \bar{C}_{R,s})d = (F + \bar{F})h.$ The total drift ratio of the system due to total lateral load $(F + \bar{F})$ can now be computed as:

$$\phi + \bar{\phi} = \left[\frac{F}{2(k_t + k_s)} + \frac{\bar{F}}{(k_t + 2k_s)} \right] \frac{h}{d^2} \tag{24}$$

Variations of tendon and sleeve forces with respect to incremental core force are presented in Figure (12d). For SS design, all tendons and sleeves should remain elastic throughout the service life of the system, i.e., $f_t \le 2f_{Y,t} / 3$, $f_s \le 2f_{Y,s} / 3$, where $f_{Y,t}$ and $f_{Y,s}$ are the yield stresses of the materials of the tendons and the sleeves, respectively. Although the sleeves are more likely to act as short columns, their slenderness ratios should also be checked for buckling, i.e., $(h_s / r_s) < \pi\sqrt{E_s / f_{Y,s}}$ or as required by the pertinent codes of practice. Moreover, if for any reason both tendons fail, then the sleeves and their connections should be strong enough to preserve the integrity of the core. With both tendons incapacitated, the sleeve will have to resist maximum reactions $C_{R,s.\max} = -C_{L,s,\max} = F_{\max} h / 2d$, in which case $A_s \ge (3F_{\max} h / 4df_{Y,s})$.

5.2.1. Pre-stressing Losses of the Sleeves

The pre-stressing losses of the sleeves can be estimated as follows. Tendon elongation due to stretching $\varepsilon_t = TL_t / A_t E_t = T / k_t$, core shortening due to compression $\varepsilon_c = CL_c / A_c E_c = C / k_c$ and $\varepsilon_s = Ch_s / A_s E_s = C / k_s$. Since $T = C$, then net tendon elongation at decompression is: $\varepsilon_u = \varepsilon_t + \varepsilon_c + \varepsilon_s = T[1/k_t + 1/k_c + 1/k_s]$. Difference between free and confined extension $= \bar{T} / k_t = \varepsilon_u - T / k_t = [T / k_t + T / k_c + T / k_s] - T / k = T / k_c + T / k_s$, $\bar{T} = [k_t / k_c + k_t / k_s]T$. Therefore, the total stressing loss is:

$$\partial T = T - \bar{T} = [1 - (k_t / k_c) - (k_t / k_s)]T \tag{25}$$

5.3. Development and Description of the Controllable REDMC

The proposed replaceable steel moment connection of Figure (4) [19] was developed to dissipate seismic energy, control locations of plastic hinges, prevent damage to the body of the beam and adjoining columns, and if needed, help prevent collapse and recenter the structure after removing the damaged flange plates. In order to prevent loss of tension due to equal gap opening and closing along the same horizontal line, X-shape tendon profiles have been used in lieu of the parallel option. Obviously, the flange plates should be designed to develop their full plastic moments of resistance for the expected seismic as well as gravity forces acting on the beam [39]. The location of the REDMCs, distance '*a*' in Figure (4), is selected under the requirements of the prevailing codes of practice in the United States. Once distance '*a*' is established, the minimum initial flange gap can be determined in such a way as to allow free rotation of the joint:

$\psi = \beta\phi$ where ϕ is the maximum plastic drift of the system and β is a geometric constant, i.e. $g \geq \beta\phi d_b / 2$. The joint splice consists of a pair of replaceable, reduced section, perforated, or prismatic flange plates and a shear tab with elongated holes at right angles to the radii of the center of rotation. The stub joint and the rest of the beam are designed to remain stable and elastic while the flange plates develop their full plastic moments of resistance. Two small U-bolts (not shown) prevent the premature, out-of-plane buckling of the flange plates. According to [40], the U-bolts can be eliminated if slenderness ratio of flange plates is limited to $Kl_p / r \leq 20$, where l_p is the distance between the first rows of the bolts on either side of the splice gap. All other components of the beam, including the shear tabs, bolt groups, welds, the pre-loaded cables, and the entire body of the beam, are expected to remain elastic throughout the loading/unloading history of the beam.

6. SS optimization and Economics

Optimization in this context implies minimum material weight, construction expediency, and minimum PERR effort. The economics of SS structures is radically different from that of conventional ERS; both the initial investment and the potential revenues of the latter systems can be wiped out due to moderate to severe earthquakes. Perhaps the most important attribute of the proposed archetype is that it can be no more costly to build than its conventional counterparts and economical to restore for routine use as intended. Since the MF of the subject archetype can be designed as an MFUS, then it would be rational to expect its total weight to be optimized. Since MFUS acts as SDOF systems, the entire frame may be assumed to be composed of imaginary rectangular modules that fit within the bays of the MF, e.g., Figure (6d). Since each imaginary module is a structure of least material weight, then the entire assembly could also be regarded as an efficient system of minimum weight. The RRC controls the distribution of forces and deformations of the MF, and the concept of drift compatible imaginary modules leads directly to the estimation of the stiffnesses of the beams and columns of the imaginary subframes of the system. This concept is further elaborated upon in case 2 below, demonstrating how PC leads to design led analysis (DLA). Parts of case 2 were adopted from [29] for modeling and verification purposes.

6.1. Case 2-Optimized Weight-Minimum Drift Association

Considering the REDMC equipped RRC-MFUS of Figure (6a) under a uniform distribution of lateral loads of intensity *F* per floor. Determining moments of inertias of beams and columns of the MF in such a way as to make it a MFUS of minimum weight is investigated.

Discussion: The static equilibrium of the RRC requires that $Q \times 4h = F(4h + 3h + 2h)$ or $Q = 9F / 4$. The free body diagram of Figure (6b) shows that the MF transfers all lateral forces to the RRC and absorbs the core reaction Q at roof level. The MF is under uniform shear Q along its height. The first, second, and third level subframe racking moments can be computed as $M_1 = 2Qh$, $M_2 = Qh$ and $M_3 = Qh$ respectively. Assuming that the MF is composed of imaginary rectangular modules that fit within the bays of the system, such as those shown in Figure (5a) and (6d), and that the location of each module is identified by the coordinate *i, j* of its upper right hand corner, then the drift $\phi_{i,j}$ of

any such module can be expressed as:

$$\phi_{i,j} = \phi = \frac{M_{i,j}}{24E}\left[\frac{h_i}{J_{i,j}} + \frac{L_j}{I_{i,j}}\right] = \frac{M_{i,j}}{K_{i,j}} \tag{26}$$

Now, if a choice is made that $K_{i,j} = K_i$ for all j, i.e., modules of constant stiffness for level i, then the racking moment of each module of level i can be estimated as $M_{i,j} = M_i / n$, which, when substituted in Equation (26), result in the values presented in Figure (6d). Since each such module is doubly symmetric, it can be regarded as a closed loop rectangular MF of minimum weight. The minimum drift-minimum weight association for closed loop rectangular frames states that "the minimum weight design of closed loop rectangular module is one involving beams and columns of equal strength and stiffness." Naturally, if the imaginary modules can be merged to form an efficient sub-frame, then the entire assembly could also be considered an efficient or minimum weight MF.

The results of the reassembled modules are summarized in Figure (6a). This strategy also results in ideal manual solutions for PERR purposes. The proposed method of generating module stiffnesses for minimal global drift is utilized further to generate module strengths for a maximum global moment of resistance. Equation (26) indicates that weight optimization can be related to a wide range of target drift ratios, starting from the elastic range up to the maximum at incipient collapse. Estimation of maximum lateral displacements at ultimate loading is a function of the envisaged method of CP and PERR. CP by itself is a function of the controlled mode of plastic failure and the corresponding deformations. The steps involved in design led analysis for CP, recentering, and post-earthquake repairs are briefly discussed through cases 3, 4, and 5 below.

6.2. Case 3-CP and PERR

Considering the RRC-MFUS of case 2, the required strengths of beams and columns of the MF are investigated in such a way to maximize the global resistance of MFUS of Figure (6a) to the external moment. The P-delta effect for convenience is ignored.

Discussion: The relative stiffnesses of Figure (6a) have been utilized as indirect guidelines for selecting the moments of resistance of the corresponding REDMCs shown in Figure (13a), where the strong column-weak beam principle has been observed by selecting $N^P > M^P$. The sequence of failure of the beams of the frame can be determined by comparing their rotational stiffnesses at incipient collapse, i.e., $\theta_{i,j} = M^P_{i,j} L_{i,j} / 6EI_{i,j} = M^P_{i,j} / 6k_{i,j}$. It may be seen that in accordance with the rules of sequential failures, beams of bay one, $j = 1$ shown in blue, will fail first, followed by simultaneous hinging of the beams of bay two, $j = 2$, shown in green, before the beams of the last bay, $j = 3$, yellow, fail simultaneously as in Figure (13b). This implies that the global incapacitation load can be computed in three incremental stages $F_u = F_1 + F_2 + F_3$. The distribution of moments of stage 1 loading F_1 is shown in Figure (13c). The sequential group failure of the bays of the MF and the corresponding drift ratios can be estimated by first computing the set of forces F_1 that cause the formation of plastic hinges in the beams of bay one. The equilibrium of stage 1 forces requires that $M_1 = \sum_{i=0}^{m}\sum_{j=1}^{n} M^P_{i,j} = 2\times 3(1+2+3+2)M^P = 48M^P = (4+3+2)F_1 h = 9F_1 h \therefore F_1 = 16M^P / 3h$. All other moments are smaller than their ultimate

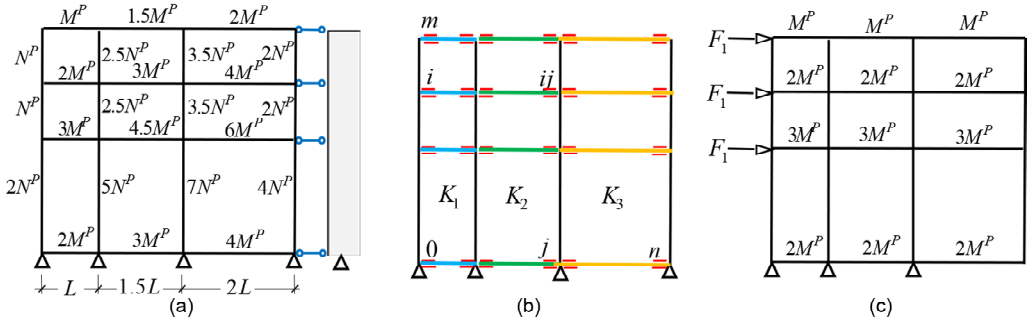

Figure 13. (a) MFUS plastic moments, (b) REDMCs and sequence of failures, and (c) Moments due to F_1.

values. Similarly, static equilibrium at incipient collapse (end of stage 3 loading) gives, $M_f = \sum_{j=1}^{n}\sum_{i=0}^{m} 2M_{i,j}^{P} = 72M^{P} = 4\lambda Qh$ or $F_u = 8M^{P}/h$. Comparing the total moments of beams of bay two, in Figures (6a) and (6c), it may be seen that for bay two moments to reach their plastic limits, the existing moment $8M^{P}$ should be increased to $12M^{P}$. This also increases bay three moments by the same amount, $4M^{P}$. The total added moment $2\times 4\times 2M^{P}$ should be compensated by $9F_2h$, i.e., $M_2 = 16M^{P} = 9F_2h$, or $F_2 = 16M^{P}/9h$. The sum of moments of bay three becomes which when $(8M^{P} + 4M^{P}) = 12M^{P}$ compared with the corresponding value in Figure (13a), needs $9F_3h$ to compensate for the deficit $2(16M^{P} - 12M^{P}) = 9F_3h$ or $F_3 = 8M^{P}/9h$. Check; $F_u = F_1 + F_2 + F_3 = (48+16+8)M^{P}/9h = 8M^{P}$, ok. Also, check $M_f = M_1 + M_2 + M_3 = (48+16+8)M^{P} = 72M^{P}$, ok.

7. Elastoplastic Displacement Analysis

Closed-form elastoplastic displacement analysis of earthquake-resisting MFs is seldom reported in the literature. However, neither CP nor PERR can be achieved without meaningful estimation of lateral deformations at first yield and/or incipient collapse. Perhaps the most remarkable feature of the proposed methodology is that it lends itself well to incremental elastoplastic displacement analysis, as demonstrated in case 4 below. Two distinct but interrelated methods of displacement analysis for well-proportioned MFUS have been devised:

a) Short hand method that takes advantage of the rules of sequential failures and deformation compatible nature of Equation (26) for any stable module at any stage of loading;
b) Long hand method that uses the Stiffness Elimination Techniques; See Appendix A.

7.1. Case 4 - Incremental Plastic Displacements

Utilizing the principles of sequential failures to compute the maximum uniform drift ratios of the MF of cases 2 and 3 at the end of each loading stage by both short and long hand methods of analysis described above.

Short hand method: Use Equation (26), and stiffness and moment data from Figures (6) and (13), respectively:

$$\phi_3 = \frac{M_{3,1}}{24E}\left[\frac{h}{J}+\frac{L}{I}\right] = \frac{4M^{P}}{K}, \quad \text{Corresponds to} \quad M = 48M^{P} \tag{27.1}$$

$$\phi_2 = \frac{M_{3,2}}{24E}\left[\frac{h}{J}+\frac{1.5L}{1.5I}\right] = \frac{4\times 1.5M^{P}}{K} = \frac{6M^{P}}{K}, \quad \text{Corresponds to} \quad M = (48+16)M^{P} = 64M^{P} \tag{27.2}$$

$$\phi_1 = \frac{M_{3,3}}{24E}\left[\frac{h}{J}+\frac{2L}{2I}\right] = \frac{4\times 2M^{P}}{K} = \frac{8M^{P}}{K}, \quad \text{Corresponds to} \quad M = (64+8)M^{P} = 72M^{P} \tag{27.3}$$

Verification of these results is presented in Appendix A. The first step in planning CP and recentering schemes is to understand the full cycle behavior of the subject earthquake resisting systems. Case 5 below utilizes the results of cases 2 and 3 to plot the $(M-\phi)$ curves of the RRC-MFUS of Figure (13a).

7.2. Case 5 - Collapse Prevention and Recentering

Determining the properties of the auxiliary devices needed to prevent collapse and achieve efficient PERR for the system of Figure (13a). The system can be treated by GSR and RFA techniques.

Discussion: The three stage idealized $(M-\phi)$ curves of the subject MF and their resultant are presented in Figure (14a), which clearly portrays the sequences of plastic collapse of the three groups of beams. The dashed black line represents the expected demand on the RCMF. Since $M > M_f$ then, the system should be strengthened utilizing wall tendons (light green line), Figure (14b), and/or other supplementary devices. Obviously, CP can be counted upon if $M_f + M_{0,t} + K_t\phi_3 > M$, a straightforward method to achieve safe CP for the present case is to select $M_{0,t} = M - M_f$. The challenge here is to use as small an initial restoring force as possible to achieve both CP and smooth PERR. Figure (14b) shows the type of response that may be expected from preloaded wall tendons. Note that $\bar{K}_1 = K_1 + K_2 + K_3$, $\bar{K}_2 = K_2 + K_3$ and $\bar{K}_3 = K_3$.

Figures (14c) and (14d) illustrate the forced and assisted recentering techniques using the same restoring moments, respectively. It may be observed that GSR was achieved by first removing group K_1 and K_3 restraints, followed by forced reversal of group K_2 members as defined in Figure (13b).

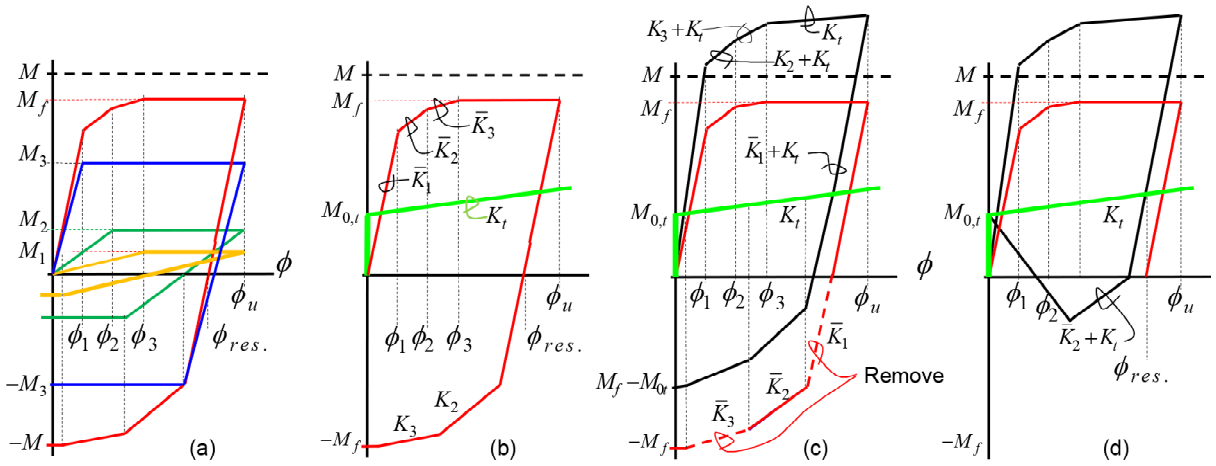

Figure 14. (a) Group responses, (b) MF and RRC response, (c) MF+RRC response, and (d) GSR response.

The small initial force overcomes the zero stiffness state of remaining system and pulls the structure back to its original location. Depending upon the size and configuration of the building under study, several recentering strategies can be considered:

Select $M_{0,t} \geq M_f$ and $K_t > 0$.

1. Large initial force, GSR and RFA not used (undesirable) (28.1)

Select $M_{0,t} \geq M_f$ and $K_t > 0$.

2. Large initial force, GSR and RFA both used (undesirable) (28.2)

Select $M_{0,t} = M - M_f$ and $K_t > 0$.

3. Minimal initial force in conjunction with GSR (desirable) (28.3)

Select $M_{0,t} = M - M_f$ and $K_t > 0$.

4. Minimal initial force, GSR and RFA not used (undesirable) (28.4)

Select $M - M_f < M_{0,t} < M_f$ and $K_t > 0$.

5. Medium force, GSR and RFA not used (undesirable) (28.5)

Select $M - M_f < M_{0,t} < M_f$ and $K_t > 0$.

6. Medium force, GSR and RFA used (desirable) (28.6)

8. Conclusions

Structures can not be regarded as seismically sustainable unless designed to remain serviceable, not collapse, with minor to moderate repairs after code-defined earthquakes. Otherwise, the system needs to be disposed with significant damage to the environment. It has been shown that damage analysis can gain insight into the practical design of earthquake resilient structural systems. It has also been demonstrated that PC can be extended to structural optimization and practical SS. SS and RCMFs are both relatively new ideas. A wealth of numerical data on the response of idealized, self-centering rocking core models, equipped with different types of repairable energy dissipating devices, has been published in the past few years. However, neither the theoretical nor practical implications of complete buildings designed for SS and incorporating RCMFs have been reported in the literature. An attempt was made in the current article to attract attention to the subject matter and to introduce preliminary design criteria for minimum-weight SS archetypes. The paper discusses a new structural archetype based on available skills, knowledge, and technologies suited for minimum-weight SSD. Some of the more important attributes of the proposed scheme can be summarized as follows:

- The proposed archetype is a structure of optimized weight and lends itself well to realignment and minimal repairs;
- The preliminary design process can be performed manually with or without auxiliary spreadsheets;
- The stabilizing tendons can be stressed or de-tensioned by means of built-in stressing jacks, turnbuckles, or other devices to assure CP and controlled PERR;
- The structure is an SDOF system. A half-cycle,

exact analysis, within the bounds of the theoretical assumptions, has been formulated through simple closed-form solutions;

- Removal of the damaged flange plates allows the joints to rotate freely until full PERR is achieved. The replacement of the REDMCs not only removes the major sources of residual displacements within the ERS but also facilitates the PERR process by reducing the stiffness of the MF to that of a partially articulated frame;
- Purpose specific detailing facilitates the PERR processes and reduces the need for large restoring forces;
- Optional gap opening high strength tendons and tensioning devices have been provided along the beams of the ERS and can be used to control the PERR process as required;
- In earthquake resisting systems of uniform response, groups of similar members, including the supplementary devices, can be identical regardless of their numbers and location within the structure;
- Recentering can be achieved by means of two newly introduced technologies, GSR and RFA, which reduce and/or adjust the magnitude of the restoring forces needed to realign the structure;
- Since the proposed archetype is a structure of minimum-weight, then material savings might offset construction costs related to the RRC and supplementary devices;
- The use of DLA addresses CP, self-alignment, reparability, and uniform drift as inherent attributes of the system;
- High strength tendons and auxiliary devices can be used to prevent actual collapse, despite the formation of damage patterns within the earthquake resisting systems;
- The RCMFs cited in this article have all passed tests of experimentations and time history analysis. Extensive computer analysis support the viability of the parametric cases presented in this paper;
- The gravity system is detailed in such a way as to neither absorb seismic energy nor accumulate residual effects.

The proposed structural schemes are still in their infancy. They are still being developed and need the test of time and scrutiny before they become viable earthquake resilient systems. Hopefully, this article will motivate others to improve and extend the proposed methodologies to develop more efficient sustainable archetypes.

9. Declarations

Funding: This research did not receive any specific grant from funding agencies in the public, commercial, or other sectors.

Conflict of interest: On behalf of all authors, the corresponding author states that there is no conflict of interest.

Availability of data and material: The authors confirm that the data supporting the findings of this study are available.

Replication of results: On behalf of all authors, the corresponding author states that the results presented in this paper can be reproduced by implementing details provided herein.

References

1. Beheshti, M. and Asadi, P. (2020) Optimal seismic retrofit of fractional viscoelastic dampers for minimum life-cycle cost of retrofitted steel frames. *Structural and Multidisciplinary Optimization*, **61**(5), 2021-2035.

2. Bohrer, R. and Kim, I.Y. (2021) Multi-material topology optimization considering isotropic and anisotropic materials combination. *Structural and Multidisciplinary Optimization*, 1-17.

3. Camacho, V.T., Horta, N., Lopes, M., and Oliveira C.S.(2020) Optimizing earthquake design of reinforced concrete bridge infrastructures based on evolutionary computation techniques. *Structural and Multidisciplinary Optimization*, **61**(3), 1087-1105.

4. Carlos Lopez, C., Burggraeve, S., Lietaert, P., Stroobants, J., Xie, X., Jonckheere, S., Pluymers, B., and Desmet, W. (2020) Model-based, multi-material topology optimization taking into account cost and manufacturability. *Structural and Multidisciplinary Optimization*, **62**(6), 2951-2973.

5. MacRae, G.A., Kimura, Y., and Roeder, C. (2004) Effect of column stiffness on braced frame seismic behavior. *Journal of Structural*

Engineering, **130**(3), 381-391.

6. Powell, G.H. (2008) Displacement-based seismic design of structures. *Earthquake Spectra*, **24**(2), 555-557.
7. Nakashima, M., Kato, H., and Takaoka, E. (1992) Development of real-time pseudo dynamic testing. *Earthquake Engineering and Structural Dynamics*, **21**(1), 79-92.
8. Eatherton, M.R., Ma, X., Krawinkler, H., Deierlein, G.G., and Hajjar, J.F. (2014) Quasi-static cyclic behavior of controlled rocking steel frames. *Journal of Structural Engineering*, **140**(11), 04014083.
9. Eatherton, M.R. and Hajjar, J.F. (2011) Residual drifts of self-centering systems including effects of ambient building resistance. *Earthquake Spectra*, **27**(3), 719-744.
10. Kawashima, K., MacRae, G.A., Hoshikuma, J.,-I., and Nagaya, K. (1998) Residual displacement response spectrum. *Journal of Structural Engineering*, **124**(5), 523-530.
11. Hajjar, J.F., Sesen, A.H., Jampole, E., and Wetherbee, A. (2013) *A Synopsis of Sustainable Structural Systems with Rocking, Selfcentering, and Articulated Energy-Dissipating Fuses*. Report No. NEU-CEE-2013-01. Dept. of Civil and Environmental Eng. Reports, Northeastern University, Boston.
12. Pollino, M., Slovenec, D., Qu, B., and Mosqueda, G. (2017) Seismic rehabilitation of concentrically braced frames using stiff rocking cores. *Journal of Structural Engineering*, **143**(9), 04017080.
13. Qu, Zh., Wada, A., Motoyui, Sh., Sakata, H., and Kishiki, Sh. (2012) Pin-supported walls for enhancing the seismic performance of building structures. *Earthquake Engineering and Structural Dynamics*, **41**(14), 2075-2091.
14. Ajrab, J.J., Pekcan, G., and Mander, J.B. (2004) Rocking wall-frame structures with supplemental tendon systems. *Journal of Structural Engineering*, **130**(6), 895-903.
15. Grigorian, C.E. and Grigorian, M. (2016) Performance control and efficient design of rocking-wall moment frames. *Journal of Structural Engineering*, **142**(2), 04015139.
16. MacRae, G.A. and Kawashima, K. (1997) Post-earthquake residual displacements of bilinear oscillators. *Earthquake Engineering and Structural Dynamics*, **26**(7), 701-716.
17. LATBSDC (2017) *An Alternative Procedure for Seismic Analysis and Design of Tall Buildings in the Los Angeles Region*.
18. Naeim, F. (2016) *New Developments in Performance-Based Seismic Design of Tall Buildings*. Los Angeles Tall Buildings Structural Design Council Conference, Los Angeles, CA, USA.
19. Grigorian, M., Moghadam, A.S., Mohammadi, H., and Kamizi, M. (2018) Methodology for developing earthquake-resilient structures. *The Structural Design of Tall and Special Buildings*, **28**(2), e1571.
20. Basagiannis, C. and Williams, M. (2017) Seismic design and evaluation of moment-resisting frames using elastomeric dampers. *6th World Conference on Earthquake Engineering, 16WCEE*. Chile.
21. Shen, Y., Christopoulos, C., Mansour, N., and Tremblay, R. (2011) Seismic design and performance of steel moment-resisting frames with nonlinear replaceable links. *Journal of Structural Engineering*, **137**(10), 1107-1117.
22. Mansour, N., Christopoulos, C., and Tremblay, R. (2011) Experimental validation of replaceable shear links for eccentrically braced steel frames. *Journal of Structural Engineering*, **137**(10), 1141-1152.
23. Wang, X., Wang, T., and Qu, Z. (2017) An experimental study of a damage-controllable plastic-hinge-supported wall structure. *Earthquake Engineering and Structural Dynamics*, **47**(3), 594-612.
24. Deirlein, G., Krawinkler, H., and Cornell, C. (2003) A framework for performance-based earthquake engineering. *Proc., 2003 Pacific Conference on Earthquake Engineering*.

25. Gebelein, J., Barnard, M., Cochran, M., Haselton, C., McLellan, R., and Porter, K. (2017) Considerations for a framework of resilient structural design for earthquakes. *2017 Seaoc Convention Procs*.

26. Grigorian, M. and Grigorian, C.E. (2018) Sustainable earthquake-resisting system. *Journal of Structural Engineering*, **144**(2), 04017199.

27. Grigorian, M., Moghadam, A., and Mohammadi, H. (2017) On rocking core-moment frame design. *16th World Conference on Earthquake Engineering, 16WCEE*, Chile.

28. Ricles, J.M., Karavasilis, S.R., and Chen, T.L. (2010) Performance-based seismic design and experimental evaluation of steel MRFs with passive dampers. *Advances in Performance-Based Earthquake Engineering*, M.N. Fardis, Editor. Springer Science and Business Media.

29. Grigorian, M. and Kamizi, M. (2021) High-performance resilient earthquake-resisting moment frames. *Proceedings of the Institution of Civil Engineers-Structures and Buildings*, 1-17.

30. Grigorian, M. and Kaveh, A. (2013) A practical weight optimization for moment frames under combined loading. *Iran University of Science and Technology*, **3**(2), 289-312.

31. Taranath, B.S. (1998) *Steel, Concrete, and Composite Design of Tall Buildings*. 2nd Ed., McGraw-Hill Professional.

32. Richard, R.H.M., Gillett, P.E., Kriegh, J.D., and Lewis, B.A. (1980) The analysis and design of single plate framing connections. *Engineering Journal*, **17**(2).

33. Astaneh, A., Call, S.M., and McMullin, K.M. (1989) Design of single-plate shear connections. *Engineering Journal*, **26**(1), 21-32.

34. Otani, S. (1997) 'Development of performance-based design methodology in Japan', in: *Seismic Design Methodologies for the Next Generation of Codes*, P. Fajfar and H. Krawinkler, Editors. Routledge, 59-67.

35. Grigorian, M. and Grigorian, C.E. (2012) Performance control: new elastic-plastic design procedure for earthquake resisting moment frames. *Journal of Structural Engineering*, **138**(6), 812-821.

36. Ma, X., Borchers, E., Krawinkler, H., Billington, G.S., Deierlein, G., and Pena, A. (2010) *Design and Behavior of Steel Shear Plates with Openings as Energy-Dissipating Fuses*. John A. Blume Earthquake Engineering Center Technical Report 173.

37. Janhunen, B. et al. (2012) Seismic retrofit of a 1960s steel moment-frame high-rise using a pivoting spine. *Proceedings of the 2012 Annual Meeting of the Los Angeles Tall Buildings Structural Design Council*.

38. Bozkurt, M.B. and Topkaya, C. (2018) Replaceable links with gusseted brace joints for eccentrically braced frames. *Soil Dynamics and Earthquake Engineering*, **115**, 305-318.

39. American Society of Civil Engineers (2010) *ASCE/SEI 7-10 in Minimum Design Loads for Buildings and Other Structures*. Reston, VA., USA.

40. Astaneh-Asl, A. (1997) *Steel Tips, Structural Steel Educational Council*. Moraga, CA., USA.

Notations & Symbols

The following symbols are used in this paper:

A_i : BRB effective cross-sectional area at level i

A_c : core cross-sectional area

a: neutral axis distance of frame to upper beam (Figure 5) code defined length of beam at each end

b: neutral axis distance of frame to lower beam (Figure 5)

$C_{L,s}$: left sleeve compression force

$C_{R,s}$: right sleeve compression force

$C_{L,s,\max}$: left sleeve maximum reaction

$C_{R,s,\max}$: right sleeve maximum reaction

d: symbolic SDOF system geometrical parameter

d_{sh}: horizontal distance between two columns

E_b: BRB modulus of elasticity

E_c: core modulus of elasticity

F_{sf}: total carrying capacity of SFs for each supporting column

f_{cr}: stability quotient
$f_{(Y,t)}$: tendon yield stress
$f_{(Y,s)}$: sleeve yield stress
G: module linearized non-plastic total weight function (Figure 5)
g: gravity acceleration
H_i: story height
h: frame geometrical parameter (Figure 5) total core height
h_e: cantilever height in symbolic SDOF system
h_s: sleeve height
h_w: height of infill wall
I: beam moment of inertia
I_L: lower beam moment of inertia
I_U: upper beam moment of inertia
J: column moment of inertia
K: stiffness effective length factor
K_B: BRB system stiffness
K_C: RRC system stiffness stretched cables stiffness (Figures 1 and 2)
K_e: elastic stiffness
K_F: frame stiffness
K_{PD}: negative stiffness due to P-delta
K_S: shear fuse system stiffness
K_T: one stretched cable stiffness (Figures 1 and 2)
k_s: sleeve axial stiffness
k_t: tendon axial stiffness
L: span length
L_c: core length
$\bar{L}_i$: BRB length at level i
l: symbolic SDOF system geometrical parameter frame geometrical parameter (Figure 5)
l_P: flange plate unbraced length
M_0: elastic moment of resistance
M_B: BRB system moment of resistance
M_C: RRC system moment of resistance
$M_{CONN.}$: bending moment acting at the base joint
M_L: lower beam end moment
M_R: total internal moment of resistance maximum restoring moment
M_{RACK}: frame total racking moment
M_U: upper beam end moment
M^P: Beam plastic moment of resistance
$\bar{M}^P$: REMDC plastic moment of resistance
M_C^E: cables elastic moment of resistance
M_{fix}^P: plastic carrying capacity of fixed base frame
M_{grd}^P: plastic carrying capacity of frame with grade beam
M_{pin}^P: plastic carrying capacity of pinned base frame
m: effective mass number of levels
N: column design moment
N^P: column moment of resistance
n: number of bays
P: gravity load
Q: roof level lateral load core reaction at roof level
R: reaction
R_0: core reaction due to tendons tension
r_s: sleeve radius of gyration
r_w: critical hole location distance to the center of rotation
T_0: cable/tendon initial tension
"T: fundamental period, earthquake-induced tensile force in cables
$T_{L,t}$: left tendon tensile force
$T_{R,t}$: right tendon tensile force
V: lateral load base shear
V_F^P: plastic load capacity of symbolic cantilever system
V_C^E: elastic shear carried by cable in symbolic cantilever system
W: gravity load
β: geometric constant (Figure 4)
γ: arbitrary constant of proportionality
Δ: lateral displacement
Δ_E: elastic lateral displacement
Δ_Y: yield lateral displacement
Δ_U: ultimate lateral displacement
Δ'_R: residual displacement
δ_F^P: Kronecker's delta
$\varepsilon_{L,s}$: left sleeve elongation
$\varepsilon_{R,s}$: right sleeve elongation
$\varepsilon_{L,t}$: left tendon elongation
$\varepsilon_{R,t}$: right tendon elongation
θ: radial inclination
θ_U: upper beam end rotation
θ_L: lower beam end rotation drift
ϕ: REDMC maximum plastic drift
ϕ_{fix}: frame drift for fixed base connection
ϕ_{grd}: frame drift with grade beam
ϕ_{max}: maximum drift
ϕ_{pin}: frame drift for pinned base connection
ϕ_Y: yield drift

Appendix A - Long hand verification of Case 3

The effect of the development of $M_{i,j}^P$ on the

response of span *ij* has been incorporated in Equation (20) by introducing Kronecker's delta $\delta_{i,j}^{P}$ and $\bar{\delta}_{i,j}^{P}$ for the individual beams and columns, res-pectively. The Kronecker's deltas $\bar{\delta}_{i,j}^{P}$ and $\delta_{i,j}^{P}$ were introduced to help track the post-earthquake unstiffening of the structure as a continuum. They refer to the effects of formation or lack of formation of plastic hinges at the ends of beams *i*, *j*. For instance $\delta_{i,j}^{P}=1$, if $M_{i,j}<M_{i,j}^{P}$, and $\delta_{i,j}^{P}=0$, if $M_{i,j}=M_{i,j}^{P}$. $\delta_{i,j}^{P}=0$ also implies structural damage or loss of stiffness with respect to member *i*, *j*. $\bar{\delta}_{i,j}^{P}$ has been introduced to include the contribution or lack of column stiffness to overall stiffness $K_{F,r}$ due to the formation of plastic hinges at the ends of the adjoining beams. For example, if the beams on either side of top and bottom ends of a column developed plastic hinges, the column would become zero, implying that $\bar{\delta}_{i,j}^{P}=0$. Use stiffness and moment data from Figures (6) and (13), respectively.

$$\text{Stage 1 } \sum k=\left[\frac{1+2+3+2}{1}+\frac{1.5+3+4.5+3}{1.5}+\frac{2+4+6+4}{2}\right]\frac{I}{L}=\frac{24I}{l},$$

$$\sum \bar{k}=\left[\frac{1+2+2+1}{1}+\frac{4+8+8+4}{2}\right]\frac{J}{h}=\frac{24J}{h}$$

$$\therefore \phi_1=\frac{9F_1h}{12E}\left[\frac{h}{24J}+\frac{L}{24I}\right]=\frac{9h}{12K}\times\frac{16M^P}{3h}=\frac{4M^P}{K}$$

$$\text{Stage 2 } \sum k=\left[\frac{2+4+6+4}{2}\right]\frac{I}{L}=\frac{8I}{l},$$

$$\sum \bar{k}=\left[\frac{1+2+1}{1}+\frac{1+2+1}{1}+\frac{4+8+4}{2}\right]\frac{J}{h}=\frac{16J}{h},$$

$$\therefore \partial\phi_2=\frac{9F_2h}{12E}\left[\frac{h}{16J}+\frac{L}{16I}\right]=\frac{9h}{K}\times\frac{16M^P}{9h}\times\frac{2}{16}=\frac{2M^P}{K}$$

and

$$\phi_2=\phi_1+\partial\phi_2=\frac{(4+2)M^P}{K}=\frac{6M^P}{K}$$